Progress In Electromagnetics Research, Vol. 130, 429–446, 2012

A RESONANCE TUNABLE AND DURABLE LSPR NANO-PARTICLE SENSOR: AL_2O_3 CAPPED SILVER NANO-DISKS

D. Mortazavi[1, *], A. Z. Kouzani[1], and K. C. Vernon[2]

[1]School of Engineering, Deakin University, Geelong, VIC 3216, Australia

[2]Applied Optics and Nanotechnology Group, Queensland University of Technology, Brisbane, QLD 4001, Australia

Abstract—Localized surface plasmon resonance (LSPR) biosensors are employed to detect target biomolecules which have particular resonance wavelengths. Accordingly, tunability of the LSPR wavelength is essential in designing LSPR devices. LSPR devices employing silver nano-particles present better efficiencies than those using other noble metals such as gold; however, silver nano-particles are easily oxidized when they come in contact with liquids, which is inevitable in biosensing applications. To attain both durability and tunabilty in a LSPR biosensor, this paper proposes alumina (Al_2O_3) capped silver nano-disks. It is shown that through controlling the thickness of the cap, the LSPR resonance frequency can be finely tuned over a wide range; and moreover, the cap protects silver nano-particles from oxidation and high temperature.

1. INTRODUCTION

Localized surface plasmon resonance (LSPR) is associated with the collective resonances at the interface of a nano-particle (NP), i.e., negative index materials (NIMs), with a background media. This resonance leads to strong electric fields on the interface between the NP and the background media at a wavelength called the LSPR wavelength. Nowadays, the applications of the surface palsmon resonance (SPR) devices are extended to utilizing metamaterials (MMs) against NIMs in microwave frequencies

Received 29 May 2012, Accepted 16 July 2012, Scheduled 21 August 2012

* Corresponding author: Daryoush Mortazavi (dmortaza@deakin.edu.au).

biosensing applications [1], and sub-wavelength single-side double-slot (SS-DS) MM and double-side double-slot (DS-DS) MM to have strong surface electric filed intensity enhancement with tuneable resonances [2]. Superlens with anti-reflection and phase control (ARPC-superlens) asymmetric structures have also been utilized in optical nano-imaging, bio-sensoring, and lithography to get super-resolution and high contrast images [3]. Moreover, an Au/Ag alloyed triangular nano-box (TNB) device has recently been used as a multifunction device in SERS biosensing and cancer drug delivery in vivo, where the femtosecond laser pulses are used to ablate the TNB and release the drug encapsulated in the TNB hollow [4]. Enhancement of the blue light emission from gallium nitride LEDs (GaN-LED) using the enhanced surface electric fields is another application, where silver metal-films are coated by n/p GaN-LED and quantum walls of the LED are in between [5].

If the NP is placed on a substrate, which is often the case in these biosensors [6–8], the resonance wavelength will be affected by the strength of the NP-substrate interaction [9]; thus, the material, shape, and physical dimension of both NP and substrate have remarkable impacts on the NP scattering, absorption, and extinction spectrum [10]. Determining this wavelength is essential in LSPR applications such as surface enhanced Raman scattering (SERS) biosensors. Biomolecules are usually Raman scatterers resonating at a particular wavelength [11]. Thus, a procedure that can be used to design LSPR devices with a desired resonance frequency is needed for a variety of application areas.

Increasing the size and elongation of NPs red-shifts the resonance wavelength and increases the enhancement. However, if the size of the NPs is comparable to the incident wavelength, multipoles are excited in addition to dipoles, which flatten the LSPR spectrum and reduce the biosensing efficiency. This flattening is due to the retardation effects where conduction electrons do not all move in phase [12, 13].

Experiments show that increasing the dielectric permittivity of the background media red-shifts the plasmon resonance causing stronger Fano resonance [14], and accordingly more enhancement. Proper design of a surrounding media is very important in design of LSPR NPs for biosensing. Noble metals that possess a negative real and a small positive imaginary dielectric constant are capable of supporting a LSPR. The most common noble metals used in LSPR applications are silver (Ag), gold (Au), copper (Cu), and aluminium (Al). Silver and gold are more common for plasmonics applications than the other metals because of their high enhancement capability in the visible wavelength ranges. Maximum SERS (surface enhanced Raman

scattering) enhancements on silver surfaces are greater than those on gold surfaces in the visible region [15]: in addition silver NPs present sharper LSPR spectrum than gold NPs due to their higher inter band threshold [16]. However, silver NPs are highly prone to oxidation and thus, have short-term stability [17]. A review on how the surrounding media, NPs morphology, and material can affect the LSPR spectrum was given by Mortazavi et al. [18].

Alumina (Al_2O_3) is an insulator with a high electrical resistivity of about $1 \times 10^{14}\,\Omega \cdot$ cm and higher dielectric constant than glass. Alumina has recently been used in LSPR devices as an adhesion layer between the NP and glass [19]. Alumina is abundant and inexhaustible, insoluble in water, and has great resistance against weathering and strong acid. It is a good thermal conductor and can reduce thermal shock resistance. In addition, it has the capability of forming in any size and shape, which is advantageous in LSPR device fabrication. A thin layer of alumina is easily formed on any exposed aluminium surface protecting it from further oxidation and high temperature [20]. Whitney et al. used atomic layer deposition (ALD) to deposit 1–600 monolayers of Al_2O_3 on silver film over nanosphere (AgFON) substrates [21]. Since alumina plays the role of a polar adsorbent, the biomolecules, particularly those with strong polarity (e.g., carboxylic acids) have a strong affinity to the alumina. Thus, another advantage of using alumina is in detecting target biomolecules [22]. Experimental investigation of the optical response of silver NPs capped with alumina dielectric using high-angle dark field microscopy has been demonstrated. The plasmonic response of the structure is highly dependent on the cap material and size as well as the NP physical dimensions [17].

Regarding the advantages of alumina, it is prudent to attempt to use this material when developing NP biosensors. In this paper we show that using Al_2O_3 we are able to modify the LSPR resonance tunabilty of the silver NPs, while providing good protection against oxidation. The wide range of LSPR resonance tunability using an alumina capped nano-disk is guaranteed by variation of the cap thickness. This feature is compared with the effect of the glass substrate thickness on LSPR resonance for nano-disks [23]. In this paper, simulations are carried out using the Finite Difference Time Domain (FDTD) method, and the results are interpreted using the analytical electrostatic eigenmode method [9, 24–26].

2. THEORETICAL BACKGROUND

Mie theory [27] is the oldest analytical method for solving the LSPR problem; however, it is restricted to spherical NP shapes. In this paper, the electrostatic eigenmode method [9] is employed to formulate the concept of image-charge for different shapes of NPs [28].

Dipole resonance modes can be investigated through the electrostatic eigenmode approximation [9, 24] where the surface plasmon resonances can be calculated using the oscillating surface charge distribution $\sigma^k(\mathbf{r_q})$ at the surface S_q denoted by the polar distance of $\mathbf{r_q}$ and the normal vector of $\hat{\mathbf{n}}$, at resonance mode k, as shown in Figure 1.

Where, $\varepsilon_m(\omega^k)$ is the permittivity of the metal at the k-th resonance frequency ω^k, and ε_b is the permittivity of the background medium.

For an arbitrary ensemble of NPs, the surface charge distributions at mode $k\sigma^k(\mathbf{r})$, can be written as a superposition of the normal modes of each NP of the ensemble as follows:

$$\sigma^k(\mathbf{r}) = \frac{\gamma^k}{2\pi} \oint \sigma^k(\mathbf{r_q}) \frac{(\mathbf{r}-\mathbf{r_q})}{|\mathbf{r}-\mathbf{r_q}|^3} \cdot \hat{\mathbf{n}} dS_q \tag{1}$$

where γ^{k} is the eigenvalue or the natural resonance of a single NP due to the charges on the surface denoted by polar distance $\mathbf{r}$, and dS_q is the differential of the surface S_{q} surrounding the NP [9, 24].

The total surface charge $\sigma(\mathbf{r})$ is calculated as the weighted summation of the surface charges at every mode k:

$$\sigma(\mathbf{r}) = \sum_k a^k\left(\omega^k\right)\sigma^k(\mathbf{r}) \tag{2}$$

where $a^k(\omega^k)$, the excitation amplitude of the k-th resonance mode is

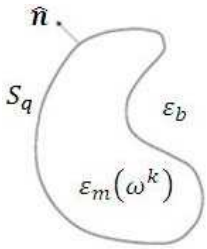

Figure 1. A particle surrounded by surface S_q.

given by:

$$a^k\left(\omega^k\right) = \frac{2\gamma^k\varepsilon_b\left(\varepsilon_m\left(\omega^k\right)-\varepsilon_b\right)}{\varepsilon_b\left(\gamma^k+1\right)+\varepsilon_m\left(\omega^k\right)\left(\gamma^k-1\right)}\mathbf{p}^k\cdot\mathbf{E}_0 \tag{3}$$

In the above equation, $\mathbf{p}^k$ is the average dipole moment of the NP at the k-th resonant mode ω^k, and $\mathbf{E}_0$ is the incident electric field amplitude.

Resonant frequency ω^k is calculated using the eigenvalue at mode k and the metal permittivity at this resonance frequency is as follows:

$$\varepsilon_m\left(\omega^k\right) = \varepsilon_b\frac{1+\gamma^k}{1-\gamma^k} \tag{4}$$

For a single spherical NP we have $\gamma^k = 3$; therefore, Eq. (4) gives the following resonance condition in a limited range of NP size which will be investigated in this paper.

$$\varepsilon_m\left(\omega^k\right) = -2\varepsilon_b \tag{5}$$

In the presence of a substrate in a background medium, the surface charges from the metal polarize both the substrate and the medium; thus, additional surface charges are created at the interface between the metal and the substrate. This phenomenon can be described by the charge-image theory [28]. As shown in Figure 2, in the charge-image theory, the combination of both substrate with electric permittivity ε_s and medium with electric permittivity ε_b (Figure 2(a)) can be considered as an infinite individual medium with an effective electric permittivity $\varepsilon_{\mathit{eff}}$ (Figure 2(b)) in which the metal NP is immersed regardless of the existence of coating on top of the NP [25].

The electric field from the surface charges of the NP in the background medium $\sigma(\mathbf{r})$ at a position $\mathbf{r}$ induces a surface charge of $\sigma(\mathbf{r_1})$ at the mirror position $\mathbf{r_1}$:

$$\sigma(\mathbf{r_1}) = \frac{\varepsilon_b-\varepsilon_s}{\varepsilon_b+\varepsilon_s}\sigma(\mathbf{r}) \tag{6}$$

This surface charge can be imagined as the surface charge on a mirror image (i.e., pseudo NP) inside the substrate, as shown in Figure 2(a) Therefore, we can assume that we have two identical interacting NPs, where electromagnetic Maxwell's equations can be analytically solved using the electrostatic eigenvalue method if the size of NPs is much less than the incident wavelength [9, 24–26]. This interaction leads to a shift in the LSPR frequency. It has been shown that in the presence of the substrate, the excitation amplitude $\tilde{a}^k(\tilde{\omega}^k)$ at the k-th mode equals to:

$$\tilde{a}^k\left(\tilde{\omega}^k\right) = \frac{2\gamma^k\varepsilon_b\left(\varepsilon_m\left(\tilde{\omega}^k\right)-\varepsilon_b\right)}{\varepsilon_b\left(\gamma^k+1\right)+\varepsilon_m\left(\tilde{\omega}^k\right)\left(\gamma^k-1\right)-\left(\varepsilon_m\left(\tilde{\omega}^k\right)-\varepsilon_b\right)\eta T^k}\mathbf{p}^k\cdot\mathbf{E}_0 \tag{7}$$

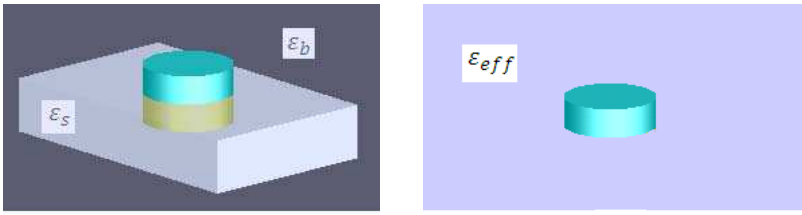

(a) (b)

Figure 2. (a) The NP in a medium with electric permittivity of ε_b (green disk on top of the substrate) and its mirror image inside the substrate with electric permittivity of ε_s (dark yellow disk inside the substrate). (b) Representation of the combined substrate/mediumshown in (a) by an infinite medium with effective permittivity of ε_{eff} in which only the NP is embedded.

where

$$\eta = \frac{\varepsilon_b - \varepsilon_s}{\varepsilon_b + \varepsilon_s} \tag{8}$$

and the interaction of the NP with the substrate is specified by the T-factor:

$$T^k = \frac{\gamma^k}{2\pi} \oint \oint \tau^k(\mathbf{r}) \frac{\hat{\mathbf{n}} \cdot (\mathbf{r} - \mathbf{r_1})}{|\mathbf{r} - \mathbf{r_1}|^3} \sigma^k(\mathbf{r_1}) \, dS dS_1 \tag{9}$$

which depends on the surface dipole eigenfunction $\tau^k(\mathbf{r})$ at the position of the NP, and surface charge eigenfunction $\sigma^k(\mathbf{r_1})$ at the position of the mirror image of the NP. The T-factor shows how strong the interaction between the NP and its mirror image is; it can be approximated by the following formula:

$$T^k = \frac{\gamma^k}{2\pi d^3} \left(3 \left(\mathbf{p}^k \cdot \hat{\mathbf{d}} \right)^2 - \mathbf{p}^k \cdot \mathbf{p}^k \right) \tag{10}$$

where $\hat{\mathbf{d}}$ is the distance vector between the centres of the NP and its mirror image in the substrate.

By comparing Eq. (3) and Eq. (7), it can be seen that the resonance frequency is changed in the presence of the substrate from ω^k to $\tilde{\omega}^k$, as if the NP is entirely immersed in a medium with dielectric permittivity of ε_{eff}:

$$\varepsilon_m \left(\tilde{\omega}^k \right) = \varepsilon_{eff} \frac{1 + \gamma^k}{1 - \gamma^k} \tag{11}$$

$$\varepsilon_{eff} = \frac{\varepsilon_m \left(\tilde{\omega}^k \right)}{\varepsilon_m \left(\omega^k \right)} = \varepsilon_b \frac{1 + \eta T^k / \left(1 + \gamma^k \right)}{1 + \eta T^k / \left(1 - \gamma^k \right)} \tag{12}$$

The polarizability of a NP with radius r, which represents a distortion of the electron cloud in response to an external electric field is calculated as follows [29]:

$$\alpha = 4\pi\varepsilon_b r^3 \frac{\varepsilon_m\left(\omega^k\right) - \varepsilon_b}{\varepsilon_m\left(\omega^k\right) + 2\varepsilon_b} \tag{13}$$

In addition, if the NP with thickness t is coated with a thin layer of dielectric of thickness d and dielectric constant ε_d, the polarizability is given by [30]:

$$\alpha = 4\pi\varepsilon_b(t+d)^3 \frac{\varepsilon_d\varepsilon_A - \varepsilon_b\varepsilon_B}{\varepsilon_d\varepsilon_A + 2\varepsilon_b\varepsilon_B} \tag{14}$$

$$\varepsilon_A = \varepsilon_m\left(\omega^k\right)(3-2P) + 2\varepsilon_d P \tag{15}$$

$$\varepsilon_B = \varepsilon_m\left(\omega^k\right)P + \varepsilon_d(3-P) \tag{16}$$

$$P = 1 - \left(\frac{t}{t+d}\right)^3 \tag{17}$$

In this paper, the advantage of using the alumina cap on tuning the resonance wavelength is proven. It is analytically explained that this advantage is due to the high dielectric constant of alumina. Alumina also has a positive impact on the protection of the silver NPs against oxidation

In addition, it is analytically shown how the physical dimensions, shape, and material type in a LSPR device can change the effective medium permittivity ε_{eff}, which in turn controls the plasmon resonance wavelength

3. SIMULATIONS AND DISCUSSIONS

The finite difference time domain (FDTD) method with PML boundary conditions [31] is used to investigate a NP on a glass substrate (see Figure 3(a)); and compared to the LSPR resonance of an NP on a glass substrate when an alumina cap is placed on top of the NP (see Figure 3(b)). In our simulations, the incident light is taken as a total field scattered field (TFSF) source [31] on the z-direction with polarization along either the x- or y-axis, which is along the elongation of the NPs, to get maximum efficiency. FDTD algorithm has capability of parallel programming implementation for very large size FDTD calculations, which will fairly speed up the modelling process [32]. In addition to the parallel processing methods, graphics processing unit (GPU) based implementation of the FDTD method offers higher

processing speed than the conventional methods in the plasmonics area while presenting the same accuracy [33].

In this modelling ε_{eff}, defined in Eq. (12), is calculated based on the reference structure of a nano-disk with radius of 40 nm and thickness of 30 nm placed on a semi-infinite glass substrate. This nano-disk structure is used as a reference to find out how increasing the thicknesses of every component in the device including the NP and the alumina cap affect the plasmon spectrum. In this simulation, only the dipole mode, i.e., the first mode, ($k = 1$) is considered; therefore, the k superscripts are no longer included in the following notes. The metal electric permittivity of the reference NP at the resonance wavelength λ is denoted by $\varepsilon_m(\lambda)$, while the resonance wavelength of the modified structures is denoted by $\tilde{\lambda}$. Here, the resonance wavelength λ corresponds to the resonance frequency ω.

Figures 4(a)–(c) indicate plasmon wavelength $\tilde{\lambda}$, ε_{eff}, and full width at half maximum (FWHM), which measures the sharpness of the spectrum, for the two structures, i.e., with and without alumina cap. The FWHM has been calculated as this gives an indication of the damping mainly due to inter band and intra band energy activation thresholds which is strongly dependent on the shape and material of the NPs.

Two cases have been considered as follows. (i) Experiment 1: The reference NP with primary thickness of 30 nm is put on the substrate and the variations of the plasmon spectrum is observed by increasing its thickness by another 0–40 nm; therefore, the thickness of the new NP structure varies within 30–70 nm. (ii) Experiment 2: The reference NP of thickness 30 nm is put on the substrate and a variable thickness alumina is capped on top of the NP where the thickness of the alumina cap is varied within 0–40 nm.

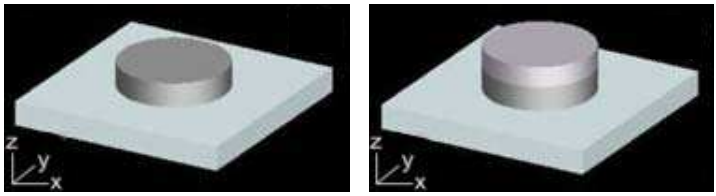

(a) (b)

Figure 3. The nano-disk structure associated with (a) glass substrate and (b) glass substrate and alumina cap on top of the NP.

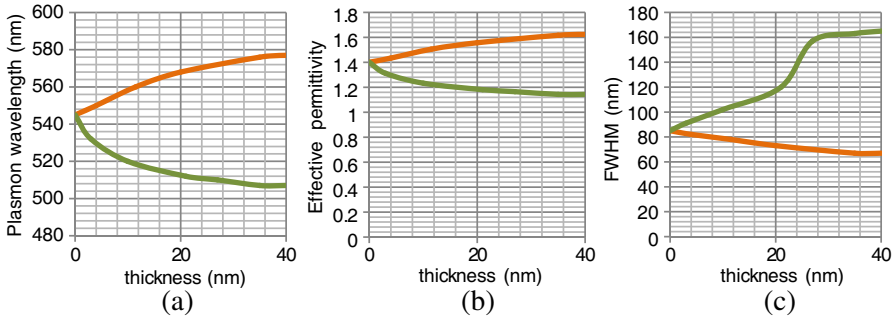

Figure 4. (a) Plasmon wavelength, (b) effective permittivity, and (c) FWHM for the nano-disk structures explained in the two experiments 1, 2 indicated by green and red colours, respectively.

3.1. Enhancement of LSPR Spectrum Factors

Figure 4 demonstrates the effect of each of the two described structures on the LSPR. The results of using the first structure are shown by green colour and for the second structure by red colour. The factors compared are the resonance wavelength (Figure 4(a)), the effective permittivity (Figure 4(b)), and the FWHM (Figure 4(c)).

These results demonstrate the following:

- The variation of the plasmon wavelength $\tilde{\lambda}$ exactly follows the variation of the effective epsilon in all cases (compare Figure 3(a) to Figure 3(b)). Since the eigenvalue γ is mostly dependent on the shape and physical dimensions of the NP, the values of $\varepsilon_m\,(\tilde{\lambda})$ and ε_{eff} are related by the constant value of γ as shown in Eqs. (1) and (2).
- The Plasmon wavelength drops and the LSPR spectrum flattens (i.e., FWHM increases) through thickening the NP (green) where NPs thicker than around 50 nm exhibit a much flattened spectrum.
- Adding a cap with higher electric permittivity than the glass substrate (e.g., alumina cap), both red-shifts the plasmon wavelength and sharpen the LSPR spectrum.

The last criterion is justified using Eqs. (14)–(17). According to Eq. (14), the plasmon resonance occurs when the denominator of the fraction approaches zero, i.e., when $\varepsilon_d\varepsilon_A = -2\varepsilon_b\varepsilon_B$. This equation can be solved for three regions as follows. (i) When there is no cap ($p = 0$), then $\varepsilon_A = 3\varepsilon_m$ and $\varepsilon_B = 3\varepsilon_d$. If these values are put in the resonant condition $\varepsilon_d\varepsilon_A = -2\varepsilon_b\varepsilon_B$, we get the known resonant condition for nano-spheres of $\varepsilon_m = -2\varepsilon_b$; (ii) when there is a thin cap ($p \approx 0$),

then according to Eqs. (15), (16) putting a cap with permittivity of ε_d on the NP results in more increase in ε_B than ε_A. To satisfy the resonant condition of $\varepsilon_d\varepsilon_A = -2\varepsilon_b\varepsilon_B$, the value of ε_A must be inevitably increased, which necessitates increasing the absolute value of ε_m which occurs at higher wavelengths. This result justifies the higher ramp in both the effective permittivity and plasmon wavelength as shown in green colour graphs in Figure 4; (iii) if there is a thick cap ($p \approx 1$), then $\varepsilon_A = \varepsilon_B = \varepsilon_m + 2\varepsilon_d$. Therefore, to realize the resonant condition $\varepsilon_d\varepsilon_A = -2\varepsilon_b\varepsilon_B$, we need to have $\varepsilon_m = -2\varepsilon_d$. Since alumina has higher permittivity than glass, the required resonant condition necessitates having higher threshold value for ε_m which occurs at higher wavelengths.

In addition, the sharpness of the LSPR spectrum is mainly due to the lower inter band activity threshold of the material used in the LSPR NPs. For example, the LSPR spectrum of silver NPs are sharper than that of the gold NPs due to the lower inter band activity threshold of silver (2 eV) than gold (3.85 eV). Since aluminium has a very low inter band activity threshold of 1.5 eV [16], putting alumina on top of the NPs enhances the sharpness of the LSPR spectrum. In addition, as shown by Sing et al. [34], a gentle breaking of the NPs symmetry, e.g., here a two layer NP, results in a weak interference between the bright and dark resonance modes [35]; therefore the creation of a sharper Fano resonance [14] was observed in our work.

3.2. Enhancement of Sensitivity and Surface Electric Fields at Hot Spots

Obviously, in the absence of a substrate, for shapes with two bases like nano-disks, the same enhancement is observed at tips along the polarization angle, i.e., along y-axis in this simulation, on both upper and lower bases. However, when putting the NP on a glass substrate, the plasmon enhancement is more pronounced at the sharp tips in the surface interface between the nano-disk and the substrate, as shown in Figure 5. This is the direct result of interaction of the NP mirror image with the original NP when using a substrate.

Besides, simulation results show that adding an alumina cap on the NP slightly enhances the scattering and the extinction cross sections at the interface between the NP and the glass substrate. Therefore, the alumina cap does not negatively affect the sensitivity of the LSPR device as a biosensor when an analyte is placed in the hot spots on the substrate; the reason is that the sensitivity in LSPR biosensors is dependent on the value of the light/matter interaction and quantified as a function of the fraction of light at the sensor surface [36]. In other research, it is also shown that putting a dielectric

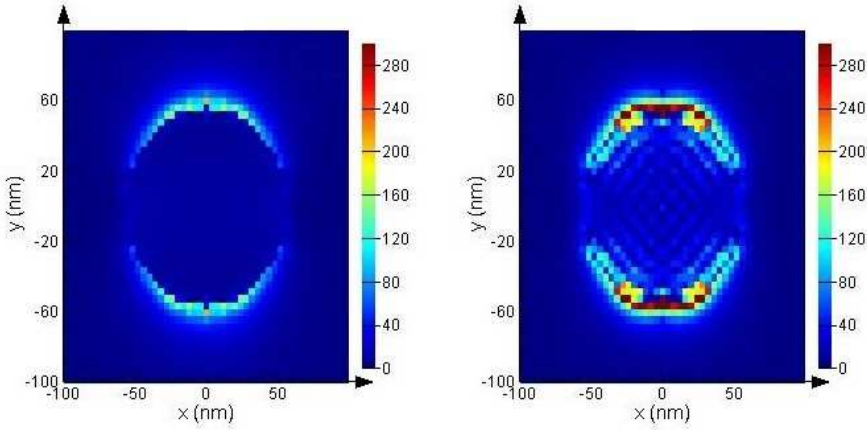

Figure 5. Total electrical field intensity on (a) plane xy on the upper base ($z = 15\,\text{nm}$) and (b) plane xy on the lower base ($z = -15\,\text{nm}$) of a nano-disk with radius of 56 nm and thickness of 30 nm on a SiO_2 substrate at resonance wavelength of 565 nm.

material with high dielectric constant on top of the NP can enhance the sensitivity of the device [37, 38]. However, because of the weak binding capacity of the glass, due to its flat surface, nano-porous alumina has recently been used to provide a greater sensitivity for gene detection; the reason is that the target molecules can be easily immobilized on the porous material [39]. In addition, phase detection method using a photo-elastic modulator can be employed in the grating-based SPR biosensors to increase the sensing sensitivity [40].

3.3. Enhancement of Resonance Wavelength Tunability

Figure 6(a) shows the variation of the plasmon wavelength versus the cap thickness as a function of the NP size. Obviously, the larger the NP is, the less effective epsilon can be attained (see Figure 6(b)); thus, the plasmon wavelength is more shifted towards red. If we assume that our background is free air with $\varepsilon_b = 1$, since for every kind of substrate $\varepsilon_s \geq 1$, then $-1 \leq \eta < 0$; therefore, $\varepsilon_s \geq \varepsilon_b = 1$. Accordingly, increasing the base size of the NPs raises the plasmon frequency and eigenvalue γ in the extrinsic regime [13]; according to Eq. (10), this will increase the T-factor due to more interaction between the NP and its mirror image, which in turn decreases ε_{eff} in Eq. (11). Regarding T and γ being positive values and η being a negative value,

we expect that $\varepsilon_{eff} \geq \varepsilon_b = 1$, where the equal sign is fulfilled for the no-substrate case ($T = 0$). Therefore, since the T-factor for high enough substrate thicknesses is independent of the substrate thickness, increasing the substrate thickness raises ε_{eff} from one towards a ceiling value according to Eqs. (9)–(12).

The proportional resonance wavelength difference between the structure in question, $\tilde{\lambda}$, and the reference NP over the substrate, λ, is defined as $\delta\lambda = (\tilde{\lambda} - \lambda)/\lambda$. This quantity is less sensitive to the NP size and has an exponential growth approaching a limit value of 0.06, as shown in Figure 6(c). Therefore, regardless of the NP size we can precisely attain around 6% increase in the plasmon wavelength, by thickening the Al_2O_3 cap from 0–40 nm. These results can be interpreted by applying the eigenmode interaction method on the charge-image theory, as explained in Section 2. According to Figure 6(c), the $\delta\lambda$ quantity for the proposed Al_2O_3 capped NP on a 30 nm-thick glass substrate is calculated as a function of the cap

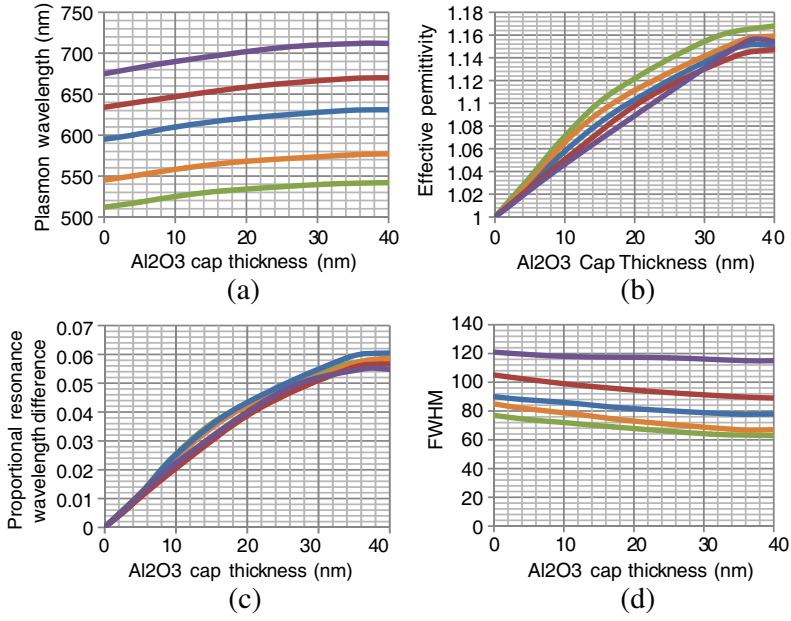

Figure 6. (a) Plasmon wavelength, (b) effective permittivity, (c) proportional plasmon wavelength difference, and (d) FWHM variations vs. the Al_2O_3 cap thickness as a function of a nano-disk with radii of 30 nm (green), 40 nm (orange), 50 nm (blue), 60 nm (brown), and 70 nm (purple), where the thickness of the NP is 30 nm.

thickness (t) and almost independent of the NP size as follows:

$$\delta\lambda(t) = 0.06\left(1 - e^{-0.055t}\right) \tag{18}$$

Another advantage of using the alumina cap is revealed from Figure 6(d). This graph explains how thickening the alumina cap will be utilized to sharpen the LSPR spectrum (i.e., smaller FWHM), while larger NPs present less sharp spectrum.

According to the definition of $\delta\lambda = (\tilde{\lambda} - \lambda)/\lambda$, it is concluded that:

$$\tilde{\lambda}(r,t) = \lambda(r) \cdot (1 + \delta\lambda(t)) \tag{19}$$

To numerically calculate the resonance wavelength of the two modified structures (Experiments 1 and 2), an estimate of the resonance wavelength of the reference NP (the individual NP with thickness of 30 nm without any alumina cap) on the glass substrate as a function of the radius of the NP is required. Figure 7 shows the variation of the resonance wavelength of the reference NP versus the radius of the NP (blue color for silica glass substrate). Accordingly, we can precisely estimate $\lambda(r)$ as a function of the radius r, $r > 20$ nm, as follows:

$$\lambda(r) = 4.1r + 388.2, \quad r > 20\,\text{nm} \tag{20}$$

Therefore, the resonance wavelength of the NP capped with alumina is formulated as a function of the size of the NP ($r \geq 20$ nm) and the thickness of the alumina cap, as follows:

$$\tilde{\lambda}(r,t) = (4.1r{+}388.2) \times \left(1 + 0.06\left(1 - e^{-0.055t}\right)\right), \quad r > 20\,\text{nm} \tag{21}$$

Figure 7 also compares the resonance wavelengths of the reference NP over silica glass with refractive index of 3.81 (blue colour), Pyrex7052 with refractive index of 5.07 (green colour), and Pyrex1710 with refractive index of 6.00 (red colour) [41]. As observed from

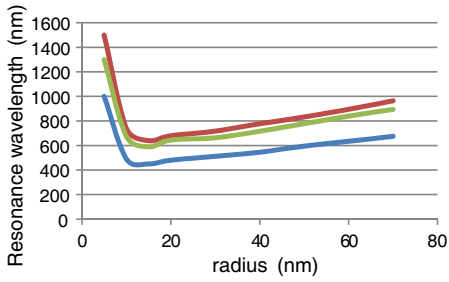

Figure 7. Plasmon wavelength of the reference NP vs. radius for silica glass (blue), Pyrex7052 (green), and Pyrex1710 (red) substrates.

Figure 7, regardless of the material of the substrate, very small NPs (i.e., NPs with radius less than 2 nm) represent another physical phenomenon in their LSPR behaviour, which is called intrinsic effect or quasi-static effect. In this range of radii, increasing the radius of the NP sharply drops the resonance wavelength. The intrinsic effect or quasi-static regime of the NP directly affects the metal permittivity $\varepsilon(r)$, while more multipoles are observed in the extinction spectrum and all the resonance peaks are very weak [13, 18]. This effect will be more pronounced for anisotropic material; where ε_m along the radial and tangential directions of the metal differ from each other. The electromagnetic simulation on a radially anisotropic cylinder demonstrates higher and sharper multipole resonance peaks than that of dipole resonance; along the radial and tangential directions of the metal differ from each other. The electromagnetic simulation on a radially anisotropic cylinder demonstrates higher and sharper multipole resonance peaks than that of dipole resonance; in addition, small changes of anisotropy shows a significant impact on the surface electric field enhancement efficiency [42].

In addition, as the radius decreases below 20 nm, the resonance wavelength blue-shifts, but it then red-shifts near 15 nm. Similar results have recently been observed by Shalabney and Abdulhalim [38] as well.

In addition, Figure 7 demonstrates that using substrates with higher refractive index red-shifts the resonance wavelength of the LSPR device. This phenomenon is revealed by Eqs. (8), (11) and (12). Accordingly, the higher is the refractive index (or permittivity) of the substrate, the longer resonance wavelength is attained. In addition, the presence of a substrate with higher permittivity results in a higher Rayleigh scattering factor; and therefore, higher surface electric field [43]. In addition, the LSPR spectrum is very dependent on the shape and aspect ratio of the NPs as recently discussed by authors in [44].

4. CONCLUSION

We investigated the effect of substrate on the LSPR spectrum for silver nano-disks. Using the image-charge theory, we concluded that putting a NP on a glass substrate causes an enhanced electric field on the interface between the NP and the substrate. We presented a new method to finely tune the resonance wavelength of the NP by placing an alumina cap on top of the NP. Thus, by finely changing the cap thickness, the resonance wavelength is precisely tuned in a wide range of wavelengths. The second advantage of utilizing the alumina cap is

in sharpening the LSPR spectrum. In addition, covering the surface of the silver NP protects it from oxidation and high temperature.

REFERENCES

1. Ishimaru, A., S. Jaruwatanadilok, and Y. Kuga, "Generalized surface plasmon resonance sensors using metamaterials and negative index materials," *Progress In Electromagnetic Research*, Vol. 51, 139–152, 2005.
2. Han, L., S. Chen, A. Schulzgen, Y. Zeng, F. Song, J.-G. Tian, and N. Peyghambarian, "Calculation and optimization of electromagnetic resonances and local intensity enhancements for plasmon metamaterials with sub-wavelength double-slots," *Progress In Electromagnetic Research*, Vol. 113, 161–177, 2011.
3. Cao, P., X. Zhang, W.-J. Kong, L. Cheng, and H. Zhang, "Super resolution enhancement for the superlens with anti-reflection and phase control coatings via surface plasmons modes of asymmetric structure," *Progress In Electromagnetic Research*, Vol. 119, 191–206, 2011.
4. Liu, X., J. Lin, T. F. Jiang, Z. F. Zhu, Q. Q. Zhan, J. Qian, and S. He, "Surface plasmon properties of hollow AuAg alloyed triangular nanoboxes and its applications in SERS imaging and potential drug delivery," *Progress In Electromagnetic Research*, Vol. 128, 35–53, 2012.
5. Zhao, J., K. Li, F. Kong, and L.-G. Du, "Enhancement of blue light emission using surface plasmons coupling with quantum wells," *Progress In Electromagnetic Research*, Vol. 108, 293–306, 2010.
6. Nath, N. and A. Chilkoti, "A colorimetric gold nanoparticle sensor to interrogate biomolecular interactions in real time on a surface," *Analytical Chemistry*, Vol. 74, 2002.
7. Samantha, S. and J. Bokatzian, "Surface plasmon resonance: Principles and applications," Graduate Student Seminar Series, Department of Chemistry, University of Alabama, 2008.
8. Homola, J., et al., "Multi-analyte surface plasmon resonance biosensing," *Methods*, Vol. 37, 26–36, 2005.
9. Davis, T. J., K. C. Vernon, and D. E. Gómez, "Designing plasmonic systems using optical coupling between nanoparticles," *Physical Review B*, Vol. 79, 155423–155432, 2009.
10. Mortazavi, D., A. Z. Kouzani, and A. Kaynak, "Nano-plasmonic biosensors: A review," *IEEE/ICME International Conference on*

Complex Medical Engineering (CME), ICMEA'11, Harbin, China, 2011.

11. Haynes, C. L., A. D. McFarland, and R. P. van Duyne, "Surface-enhanced Raman spectroscopy," *Analytical Chemistry*, Vol. 77, 339–346, Sep. 1, 2005.
12. Maier, S. A. and H. A. Atwater, "Plasmonics: Localization and guiding of electromagnetic energy in metal/dielectric structures," *J. of Applied Physics*, Vol. 98, 2005.
13. Link, S. and M. A. El-Sayed, "Spectral properties and relaxation dynamics of surface plasmon electronic oscillations in gold and silver nanodots and nanorods," *J. Physical Chemistry B*, Vol. 103, 8410–8426, 1999.
14. Zhang, S., et al., "Substrate-induced fano resonances of a plasmonic nanocube: A route to increased-sensitivity localized surface Plasmon resonance sensors revealed," *Nano Letters*, Vol. 11, 1657–1663, 2011.
15. Stuart, D. A., et al., "Glucose sensing using near-infrared surface-enhanced raman spectroscopy: Gold surfaces, 10-day stability, and improved accuracy," *Analytical Chemistry*, Vol. 77, 4013–4019, 2005.
16. Sekhon, J. S. and S. S. Verma, "Rational selection of nanorod plasmons: Material, size, and shape dependence mechanism for optical sensors," *Plasmonics*, 1–7, 2012.
17. Lantiat, D., et al., "Evidence for capping-layer effects on the morphology and plasmon excitation of Ag nanoparticles," *J. of Applied Physics*, Vol. 102, 2007.
18. Mortazavi, D., A. Z. Kouzani, A. Kaynak, and W. Duan, "Developing LSPR design guidlines," *Progress In Electromagnetic Research*, Vol. 126, 203–235, 2012.
19. Niu, J., et al., "Graphene induced tunability of the surface plasmon resonance," *Applied Physics Letters*, Vol. 100, 2012.
20. Elert, G., "Resistivity of aluminum oxide," *The Physics Factbook*, E. Huang (ed.), http://hypertextbook.com/facts/2006/EuniceHuang.shtml, 2006.
21. Whitney, A. V., et al., "Localized surface plasmon resonance nanosensor: A high-resolution distance-dependence study using atomic layer deposition," *J. Physical Chemistry B*, Vol. 109, 20522–20528, 2005.
22. Zhang, X., et al., "Ultrastable substrates for surface-enhanced Raman spectroscopy: Al_2O_3 overlayers fabricated by atomic layer deposition yield improved anthrax biomarker detection,"

American Chemical Society, Vol. 128, 10304–10309, 2006.

23. Mortazavi, D., A. Z. Kouzani, and A. Kaynak, "Investigating nanoparticle-substrate interaction in LSPR biosensing using the image-charge theory," *EMBC'12*, San Diego, USA, Aug. 2012.
24. Davis, T. J., D. E. Gomez, and K. C. Vernon, "Simple model for the hybridization of surface plasmon resonances in metallic nanoparticles," *Nano Letters*, Vol. 10, 2618–2625, 2010.
25. Vernon, K. C., et al., "Influence of particle-substrate interaction on localized plasmon resonances," *Nano Letters*, Vol. 10, 2080–2086, 2010.
26. Gómez, D. E., K. C. Vernon, and T. J. Davis, "Symmetry effects on the optical coupling between plasmonic nanoparticles with applications to hierarchical structures," *Physical Review B*, Vol. 81, 075414-423, 2010.
27. Mishchenko, M. I., L. D. Travis, and J. W. Hovenier, *Light Scattering by Nonspherical Particles: Theory, Measurements, and Applications*, Academic Press, 2000.
28. Yamaguchi, T., S. Yoshida, and A. Kinbara, "Optical effect of the substrate on the anomalous absorption of aggregated silver films," *Thin Solid Films*, Vol. 21, 173–187, 1974.
29. Lee, B., et al., "Review on subwavelength confinement of light with plasmonics," *J. of Modern Optics*, Vol. 57, 1479–1497, 2010.
30. Petryayeva, E. and U. J. Krull, "Localized surface plasmon resonance: Nanostructures, bioassays and biosensing — A review," *Analytica Chimica Acta*, Vol. 706, 8–24, 2011.
31. Taflove, A., *Computational Electrodynamics: The Finite-difference Time-domain Method*, Artech House, London, Boston, 1995.
32. Vaccari, A., A. Cala' Lesina, L. Cristoforetti, and R. Pontalti, "Parallel implementation of a 3D subgriding FDTD algorithm for large simulations," *Progress In Electromagnetic Research*, Vol. 120, 263–292, 2011.
33. Lee, K. H., I. Ahmed, R. S. M. Goh, E. H. Khoo, E. P. Li, and T. G. G. Hung, "Implementation of the FDTD method based on Lorentz-Drude dispersive model on GPU fro plasmonics applications," *Progress In Electromagnetic Research*, Vol. 116, 441–456, 2011.
34. Singh, R., et al., "Sharp fano resonances in THz metamaterials," *Optics Express*, Vol. 19, 6312–6319, 2011.
35. Zhang, W., B. Gallinet, and O. J. F. Martin, "Symmetry and selection rules for localized surface plasmon resonances in

nanostructures," *Physical Review B*, Vol. 81, 233407–233410, 2010.

36. Fan, X., et al., "Sensitive optical biosensors for unlabeled targets: A review," *Analytica Chimica Acta*, Vol. 620, 8–26, 2008.
37. Lahav, A., M. Auslender, and I. Abdulhalim, "Sensitivity enhancement of guided-wave surface-plasmon resonance sensors," *Optics Letters*, Vol. 33, 2539–2541, 2008.
38. Shalabney, A. and I. Abdulhalim, "Sensitivity-enhancement methods for surface plasmon sensors," *Laser & Photonics Reviews*, Vol. 5, 571–606, 2011.
39. Kang, M., et al., "Protein capture in silica nanotube membrane 3-D microwell arrays," *Anal. Chem.*, Vol. 77, 6243–6249, 2005.
40. Luo, Z., T. Suyama, X. Xu, and Y. Okuno, "A grating-based plasmon biosensor with high resolution," *Progress In Electromagnetic Research*, Vol. 118, 527–539, 2011.
41. Lide, D. R., *CRC Handbook of Chemistry and Physics*, 87th Edition, Taylor and Francis Group, Boca Raton, FL, 2007.
42. Jin, Y., D. Gao, and L. Gao, "Plasmonic resonant light scattering by a cylinder with radial anisotropy," *Progress In Electromagnetic Research*, Vol. 106, 335–347, 2010.
43. Kuwata, H., et al., "Resonant light scattering from metal nanoparticles: Practical analysis beyond Rayleigh approximation," *Applied Physics Letters*, Vol. 83, 4625–4627, 2003.
44. Mortazavi, D., et al., "Plasmon eignevalues as a function of nanospheroids size and elongation," *Proceeding of ICMEA'12*, Kobe, Japan, Jul. 2012.